Formation, stabilities, and electronic properties of nitrogen defects in graphene

Yoshitaka Fujimoto and Susumu Saito
Department of Physics, Tokyo Institute of Technology, Oh-okayama, Meguro, Tokyo 152-8551, Japan
(Received 25 March 2011; published 27 December 2011)

We investigate nitrogen-doping effects in a graphene sheet using a first-principles electronic-structure study in the framework of density-functional theory. As possible configurations of nitrogen impurities in graphene, substitutional nitrogen and pyridine-type defects around a monovacancy and around a divacancy are considered, and their energetics and electronic structures are discussed. The formation-energy calculations suggest that substitutional doping of the nitrogen atom into a graphene sheet is energetically the most favorable among the possible nitrogen-doping configurations. Furthermore, by comparison of the total energy of the pyridine-type defects with that of the substitutional nitrogen defect in graphene, it is revealed that formation of the pyridine-type defects becomes energetically favorable compared with formation of the substitutional nitrogen defect in the presence of a vacancy. From the results of electronic-band-structure calculations, it is found that the nitrogen-impurity states appear around the Fermi level as either acceptorlike or donorlike states, depending on the atomic geometries of the nitrogen impurities in graphene. We also calculate the scanning tunneling microscopy (STM) images associated with impurity-induced electronic states for future experimental identification of nitrogen impurities. The simulated STM images of the three N-doping configurations considered here are found to be strongly dependent on the local density of states around the nitrogen impurity, and therefore the doping configurations should be distinguishable from one another. The similarities and differences of the electronic structures and STM corrugations between N-doped and undoped graphenes are also discussed.

DOI: 10.1103/PhysRevB.84.245446 PACS number(s): 73.22.Pr, 73.20.Hb, 71.15.Mb

I. INTRODUCTION

Graphene, a single sheet of a hexagonal carbon network, has attracted much attention because it shows unique electronic properties, such as massless Dirac fermion behaviors and high carrier mobility in spite of its monatomic-layer geometry.[1–3] The recent experimental realization of a graphene sheet was, therefore, a breakthrough in the field of next-generation carbon-based nanoelectronics.[4] Modifications of the geometric and electronic structures of graphene are expected to lead to further discoveries of new electronic properties and fabrication of novel graphene-based materials.

One of the most accessible methods to tailor the electronic properties of graphenes should be the doping of foreign atoms into its honeycomb carbon network. Specifically, nitrogen is one of the most efficient dopants for carbon-based materials. In general, the doping of nitrogen substitutionally into carbon-based materials is expected to yield a donor state in their electronic structures. It is known that substitutional nitrogen doping into the C_{60} cage as well as into diamond induces donor states.[5,6] Recent experimental measurements of x-ray photoelectron spectra of N-doped graphene as well as N-doped carbon nanotubes have revealed the existence of several N-doped configurations.[7–10] It has been reported theoretically that the structural variety of nitrogen defects in carbon nanotubes provides rich electronic properties such as *p*-type and *n*-type conductivity depending on how the N-doped configurations are formed.[11,12] However, theoretical research on nitrogen doping into graphene is still limited at present. In order to manipulate the electronic properties of graphene by doping, it is of essential importance to understand the formation processes and the stabilities of N-related defects in graphene and the properties of the electron states near the Fermi level associated with these defects.

In this paper, we report on a first-principles electronic-structure study that clarifies the relationship among atomic structures, energetics, and electronic properties of nitrogen defects in graphene. We examine the possible atomic configurations of the nitrogen defects in graphene and discuss the energetics of the N-doped defects by addressing two different quantities: the *formation energy* and the *relative energy*. Scanning tunneling microscopy (STM) images are demonstrated to reveal the relationship between the atomic configurations and spatial distributions of electronic states associated with N-doping defects in graphene. It is found that STM images of several N-doped configurations in graphene clearly show distinctive corrugations reflecting the atomic geometries around the defects.

The paper is organized as follows. In Sec. II, we describe the computational methodology and calculational details. The energetics, the electronic structures, and the scanning tunneling microscopy images of nitrogen defects in graphene are discussed in Sec. III. Finally, we summarize this work in Sec. IV.

II. STRUCTURAL CONFIGURATIONS CONSIDERED AND COMPUTATIONAL METHODS

We consider five model configurations for N-doped graphene and two configurations for undoped defective graphene in order to discuss the energetics and electronic properties resulting from nitrogen doping into graphene. To simulate both N-doped and undoped but defective graphenes as isolated systems, we chose a 4×4 supercell oriented along directions parallel to the graphene sheet.[13] The geometries of the N-doped and undoped graphenes considered are illustrated in Figs. 1(a)–1(e) and 1(f) and 1(g), respectively. In Fig. 1(a), substitutionally nitrogen-doped graphene ($C_{31}N$) is shown,

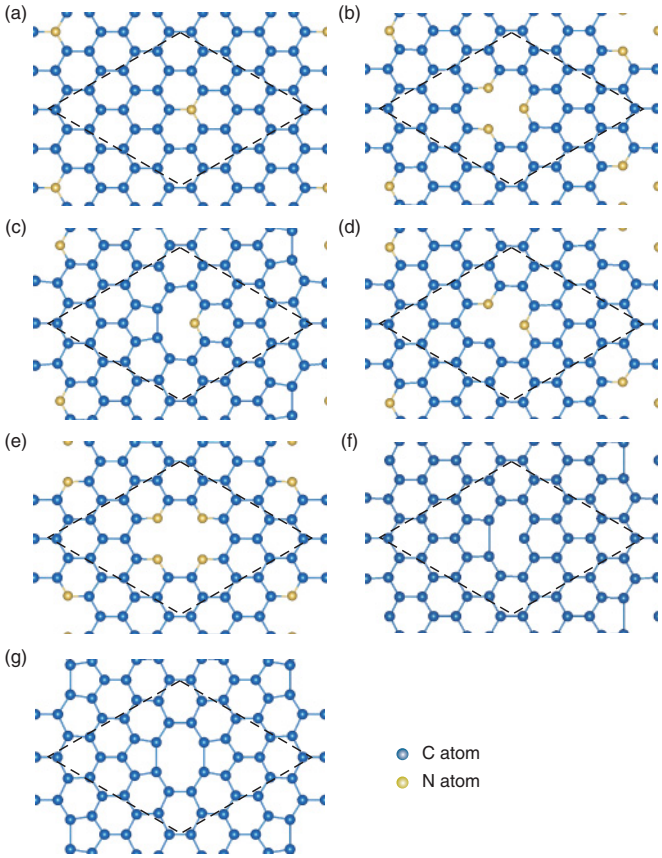

FIG. 1. (Color online) Atomic configurations of the N-doped graphenes and undoped but defective graphenes considered: (a) substitutional nitrogen defect ($C_{31}N$), (b) trimerized pyridine-type defect ($C_{28}N_3$), (c) monomeric pyridine-type defect ($C_{30}N$), (d) dimerized pyridine-type defect ($C_{29}N_2$), (e) tetramerized pyridine-type defect ($C_{26}N_4$), (f) a monovacancy (C_{31}), and (g) a divacancy (C_{30}). In each case, the geometry is fully optimized in the framework of density-functional theory (see text). The dashed lines show the supercell.

where one C atom is replaced with a N atom. As pyridine-type configurations around a monovacancy, trimerized ($C_{28}N_3$), monomeric ($C_{30}N$), and dimerized ($C_{29}N_2$) defects are illustrated in Figs. 1(b)–1(d). In addition, a tetramerized pyridine-type configuration ($C_{26}N_4$) is also shown in Fig. 1(e), where four N atoms are arranged around a divacancy. In Figs. 1(f) and 1(g), we show undoped but defective graphenes with a monovacancy (C_{31}) and a divacancy (C_{30}), respectively.

We perform first-principles total-energy calculations within the framework of density-functional theory.[14] The interactions between the ions and the valence electrons are described by norm-conserving Troullier-Martins pseudopotentials,[15] and exchange-correlation effects are treated using the local-density approximation (LDA) parametrized by Perdew and Zunger.[16,17] Wave functions in the Kohn-Sham equations are expanded in terms of a plane-wave basis set with the cutoff energy of 50 Ry.[18] The vacuum region of the supercell along the direction perpendicular to the graphene sheet is set to be 12 Å. The Brillouin-zone integration is performed with $6 \times 6 \times 1$ k-point sampling. Upon geometry optimization, the atomic configurations are updated until Hellmann-Feynman forces on all atoms are less than 0.05 eV/Å. The geometries shown in Fig. 1 are the geometries optimized in this manner. In addition to the LDA calculations, we have also performed electronic-structure calculations using the local-spin-density approximation[16,17] for the geometries optimized by the LDA in order to study the magnetic moments of the N-doped graphenes.

To discuss the energetics of nitrogen doping, we define the formation energy $E_f = E_{tot} - m_C\mu_C - m_N\mu_N$, where E_{tot} is the total energy of the N-doped graphene, m_C and m_N are the numbers of C and N atoms in a supercell, respectively, and μ_C and μ_N are the chemical potentials of the C and N atoms using pristine graphene and the N_2 molecule respectively as reference systems.

To further discuss the relative stabilities of N-doped graphenes, we also define the relative energies as

$$E_1 = E_{tot}(C_{28}N_3) + E_{tot}(C_{32}) \times 3 - [E_{tot}(C_{31}N) \times 3 + E_{tot}(C_{31})], \quad (1)$$

$$E_2 = E_{tot}(C_{28}N_3) + E_{tot}(C_{32}) \times 3 - [E_{tot}(C_{31}N) \times 3 + E_{tot}(C_{30}) + E_{tot}(C_1)], \quad (2)$$

$$E_3 = E_{tot}(C_{28}N_3) + E_{tot}(C_{32}) \times 2 - [E_{tot}(C_{31}N) \times 2 + E_{tot}(C_{30}N)], \quad (3)$$

$$E_4 = E_{tot}(C_{28}N_3) + E_{tot}(C_{32}) - [E_{tot}(C_{31}N) + E_{tot}(C_{29}N_2)]. \quad (4)$$

Here, $E_{tot}(C_{32})$, $E_{tot}(C_{31})$, and $E_{tot}(C_{30})$ are the total energies of pristine graphene, undoped graphene with a monovacancy, and undoped graphene with a divacancy, respectively, and $E_{tot}(C_{28}N_3)$, $E_{tot}(C_{29}N_2)$, $E_{tot}(C_{30}N)$, and $E_{tot}(C_{31}N)$ are the total energies of N-doped graphenes with trimerized, dimerized, and monomeric pyridine-type defects and a substitutional N-doped defect, respectively. $E_{tot}(C_1)$ is the energy per atom in pristine graphene, which is the same as the chemical potential μ_C defined above.

The STM images of various graphene sheets are constructed under the Tersoff-Hamann approximation.[19] Although it is expressed in a simple form, the method is widely used and is well known to be valid for many systems.[20–23] In this method, it is assumed that the tunneling current is proportional to the local density of states (LDOS) of the surface at the tip position integrated over an energy range restricted by the applied bias voltage. Consequently, the STM images can be generated from the isosurface of the spatial distribution by integration of the LDOS $\rho(x,y,z;\epsilon)$ at spatial points (x,y,z) and energy ϵ by sampling several k points of the Brillouin zone over the energy range from the Fermi energy E_F to $E_F - \mathrm{eV}$ with applied voltage V, i.e., $\int_0^{\mathrm{eV}} \rho(x,y,z;E_F - \mathrm{eV} + \epsilon)d\epsilon$. Thereby the calculated STM images should correspond to experimental constant-current images.

III. RESULTS AND DISCUSSION

A. Structure

To discuss their structure and stability, structural optimizations of various N-doped and undoped but defective graphenes are performed based on the local-density approximation within

density-functional theory (Fig. 1). Before discussing nitrogen defects in graphene, we show the optimized pristine graphene. Our calculated lattice constant for pristine graphene is 2.44 Å, which is in good agreement with the experimental value of 2.46 Å.[24] It also agrees with reported calculated lattice constant values and bond lengths.[24–26]

We here study the structural properties of the substitutional nitrogen defect where one C atom is replaced by a N atom [Fig. 1(a)]. The C–N bond length of the substitutional N defect in graphene is found to be 1.40 Å, which is slightly shorter than the C–C bond length of 1.41 Å in pristine graphene calculated with the same methodology. In addition, it is noted that the N atom seems to be in a planar sp^2-bonding configuration.

We next study N-doped graphene with a monovacancy, where one C atom is removed. For trimerized pyridine-type graphene, the N atom is twofold coordinated with the C–N bond length of 1.33 Å [Fig. 1(b)]. This is much shorter than the C–C bond length of the pristine graphene sheet. To obtain more insight into this vacancy–substitutional-defect complex, we consider the undoped graphene with a monovacancy. In this case, the relaxation around the vacancy can be considered to proceed as a Jahn-Teller distortion since the symmetry around the vacancy is lowered from D_{3h} to C_s. As a result, two of the three C atoms around the vacancy approach each other, forming a pentagonlike structure [Fig. 1(f)].[21,22] However, the distance apart of these two C atoms is relatively long compared with the C–C bond length of pristine graphene.[26] This implies that the interaction between the two C atoms could be relatively weak. On the other hand, although the three N atoms in the defect region move away from one another [Fig. 1(b)], the trimerized pyridine-type defect preserves D_{3h} symmetry.

So far, only the trimerized pyridine-type defect has been treated. We now consider monomeric and dimerized pyridine-type configurations around a monovacancy. In the monomeric pyridine-type defect formation [Fig. 1(c)], two C atoms around the monovacancy also move so close as to form a covalent bond. This behavior is similar to that around the monovacancy in undoped graphene, as discussed above. In the case of the dimerized pyridine-type defect formation [Fig. 1(d)], one C atom around the monovacancy has one sp^2 dangling bond since the distance between the C atom and the N atom around the monovacancy is large, approximately 2.46 Å. This is different from the case of N-doped (10,0) carbon nanotubes where a C–N bond is formed around the vacancy. The difference may be caused by curvature effects in carbon nanotubes.[12]

We also study N-doped graphene with a divacancy where two C atoms are removed. In this structure, there are tetramerized pyridine-type defects around the divacancy [Fig. 1(e)]. After the structural optimization, the C–N bond lengths are found to be within the range 1.32–1.33 Åand the interatomic distances among the four N atoms remain very long, as in the case of trimerized pyridine-type defects. On the other hand, for undoped graphene with a divacancy, the neighboring C atoms around the divacancy come close together, leading to pentagon-octagon-pentagon formation after structural relaxation of the divacancy [Fig. 1(g)]. Thus, C atoms around the divacancy prefer the configuration of the C–C bond to saturate dangling bonds, whereas formation of a N–N bond around the vacancy seems to be unfavorable.

TABLE I. Calculated formation energies of N-doped graphene. See Fig. 1 for the five structures considered here.

Formation energy (eV)				
$E_f(C_{31}N)$	$E_f(C_{28}N_3)$	$E_f(C_{26}N_4)$	$E_f(C_{30}N)$	$E_f(C_{29}N_2)$
0.32	2.51	2.55	5.61	4.28

B. Energetics

To discuss the energetics of various N-doped graphenes, we now calculate the formation energies E_f. Table I shows the calculated formation energies. The formation energy of the substitutional N-doped graphene is found to be lowest, 0.32 eV. For N-doped graphenes with a vacancy, our calculations show that the most stable configuration is the trimerized pyridine-type defect (2.51 eV), while the formation energy of the tetramerized pyridine-type defect is 2.55 eV. The energy difference between these pyridine-type configurations is only 0.04 eV. This small difference implies the existence of both defects, and they are both candidates for pyridine-type configurations in graphene. Our results for the formation energy are similar to those in previous reports.[27–29]

We further extend our discussion of the energetics of N-doped graphenes. The formation energy discussed above implies an energetic preference for nitrogen doping into the perfect graphene sheet. On the other hand, to address how the pyridine-type configurations are formed, we discuss the relative energies defined in Eqs. (1)–(4) which compare the total energy of the trimerized pyridine-type configurations directly with that of the substitutional configuration. As can be seen from the definitions of E_1 and E_2 [Eqs. (1) and (2)], the E_1 and E_2 values clarify the energetic preferences in the presence of a monovacancy and a divacancy in graphene, while with E_3 and E_4, we consider the energetic preferences in the presence of monomeric and dimerized pyridine-type defects, respectively.

The calculated relative energies of N-doped graphenes are listed in Table II. From the results for the relative energy E_1, the trimerized pyridine-type configuration is favored by 6.76 eV in energy compared with the substitutional nitrogen configuration when a monovacancy defect exists in graphene. In the presence of a divacancy, the trimerized pyridine-type configuration is also energetically preferred, $E_2 = -7.13$ eV. We next consider the relative energies E_3 and E_4 defined by Eqs. (3) and (4), corresponding to the growth processes of the monomeric and dimerized pyridine-type defects into trimerized pyridine-type defects. The E_3 value of -3.75 eV means that the monomeric configuration is less stable than the trimerized one by 3.75 eV if two substitutional nitrogen defects are also present and can react with the monomeric

TABLE II. Calculated relative energies of N-doped graphenes. The relative energies E_1–E_4 are defined in Eqs. (1)–(4), respectively.

Relative energy (eV)			
E_1	E_2	E_3	E_4
−6.76	−7.13	−3.75	−2.10

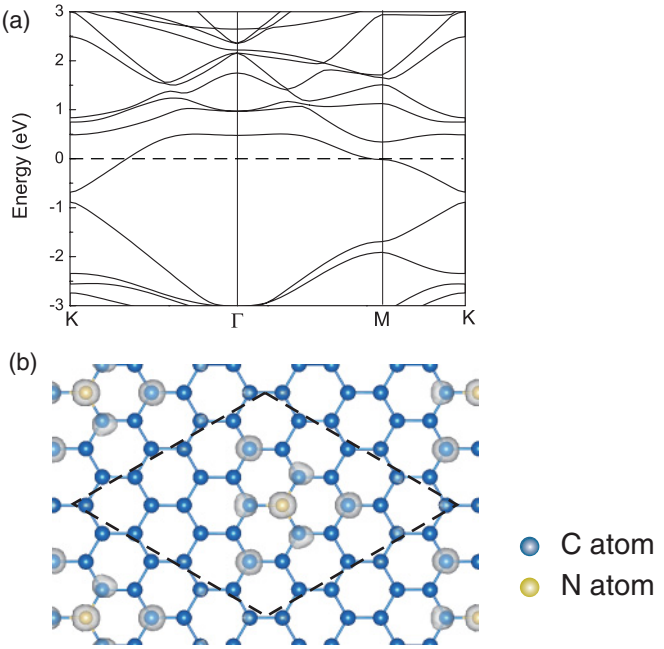

FIG. 2. (Color online) (a) Energy band and (b) isosurface of electron density of substitutional nitrogen defect in graphene (see text). The isosurface value of the electron density is set to 0.03 electron/Å^3. The Fermi energy is set to zero. The dashed lines show the supercell.

pyridine-type defect. In the case of relative energy $E_4 = -2.10$ eV, the dimerized nitrogen formation is also less stable than the trimerized one by 2.10 eV. We thus find that trimerized pyridine-type defect formation is more favorable in energy than substitutional nitrogen defect formation when a vacancy exists in graphene. Furthermore, the trimerized pyridine-type defect formation is found to be energetically preferred compared with the monomeric and dimerized forms.

C. Energy bands and electronic states

We examine the electronic structures of supercells of defective graphenes with substitutional nitrogen [Fig. 1(a)] and trimerized [Fig. 1(b)] and tetramerized pyridine-type [Fig. 1(e)] defects. In the case of substitutionally N-doped graphene shown in Fig. 2(a), the substitutional N-impurity state is observed below the conduction-band bottom. The substitutionally N-doped graphene thus may possess *n*-type conductivity since the N atom has one extra electron compared with the C atom. In Fig. 2(b), the isosurface of electron density of substitutionally N-doped graphene at the Γ point is displayed. The electron density of the nitrogen impurity is delocalized around the N atom. Interestingly, this delocalization in the electron density is also observed in other defects with threefold symmetry, such as impurity-doped and impurity-adsorbed graphenes.[32–34]

The energy bands of graphene with trimerized pyridine-type defects are shown in Fig. 3(a). In contrast to the case of substitutional nitrogen doping, here the impurity -induced states reside inside the valence band of graphene. This is because the number of electrons of trimerized pyridine-type defective graphene is less than in pristine graphene. The electron deficiency gives rise to an acceptor-type level, and the trimerized pyridine-type graphene should exhibit *p*-type conducting behavior. It is observed that there exist three impurity states near the Fermi level. In Figs. 3(b)–3(d), we show the isosurfaces of electronic states of a single state and two degenerate states at the Γ point, respectively. It is interesting to note that the features of impurity states of the trimerized

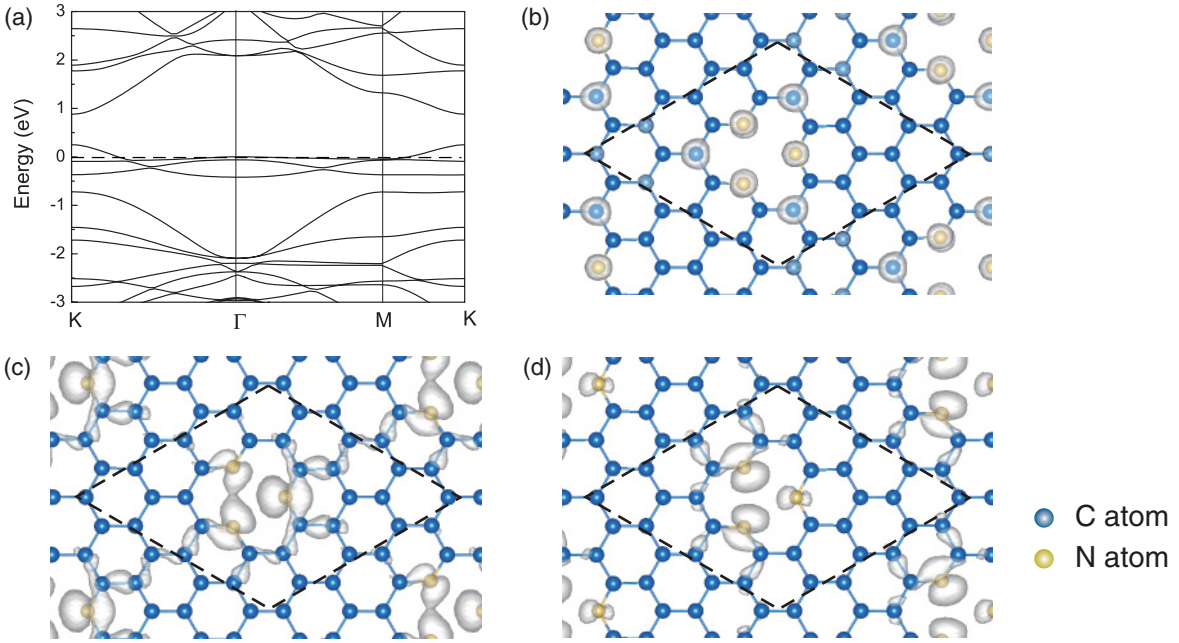

FIG. 3. (Color online) (a) Energy band and (b)–(d) isosurfaces of electron densities of the three states associated with trimerized pyridine-type defects in graphene (see text). The isosurface value of the electron density is set to 0.03 electron/Å^3. The Fermi energy is set to zero. The dashed lines show the supercell.

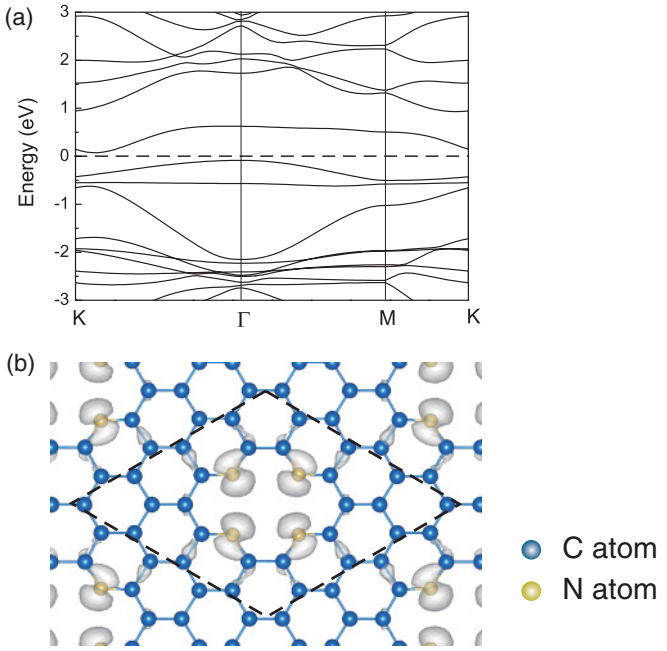

FIG. 4. (Color online) (a) Energy band and (b) isosurface of electron density of tetramerized pyridine-type defects in graphene (see text). The isosurface value of the electron density is set to 0.03 electron/Å^3. The Fermi energy is set to zero. The dashed lines show the supercell.

pyridine-type defect are similar to those of the unrelaxed structure of undoped graphene with a monovacancy.[21]

Figures 4(a) and 4(b) illustrate respectively the energy band and the isosurface of electron density of the valence-band top at the Γ point of graphene with tetramerized pyridine-type defects. There are several nitrogen-related impurity states near the Fermi level, as in the case of the trimerized pyridine-type defects in graphene. Figure 4(b) shows that the impurity state is spatially localized around the divacancy and it forms *p*-like orbital shapes localized at N atoms.

We have studied the magnetic moments of the N-doped graphenes shown in Figs. 1(a)–1(e), based on spin-polarized density-functional theory. Interestingly, we find that the trimerized pyridine-type defective graphene [Fig. 1(b)] has a magnetic moment of 0.89 μ_B. The magnetic moments of other N-doped graphenes are found to be zero. The total energy difference between spin-polarized and spin-unpolarized calculations of graphene with trimerized pyridine-type defects is 0.02 eV. This suggests that the trimerized pyridine-type defective graphene has a magnetic moment at low temperature. Thus, the trimerized pyridine-type defect might be useful as a source of magnetism in graphene at low temperatures.

D. Scanning tunneling microscopy images

Figure 5 shows STM images of N-impurity defects in graphene. In Fig. 5(a), the STM image of substitutional N-doped graphene at a bias voltage of +0.5 eV (conduction band) is shown. Three bright protrusions are seen at the three C atoms around the N atom. The dark area in the STM image is located above the N atom as if the N atom were absent, although the spatial distribution of the impurity-induced state

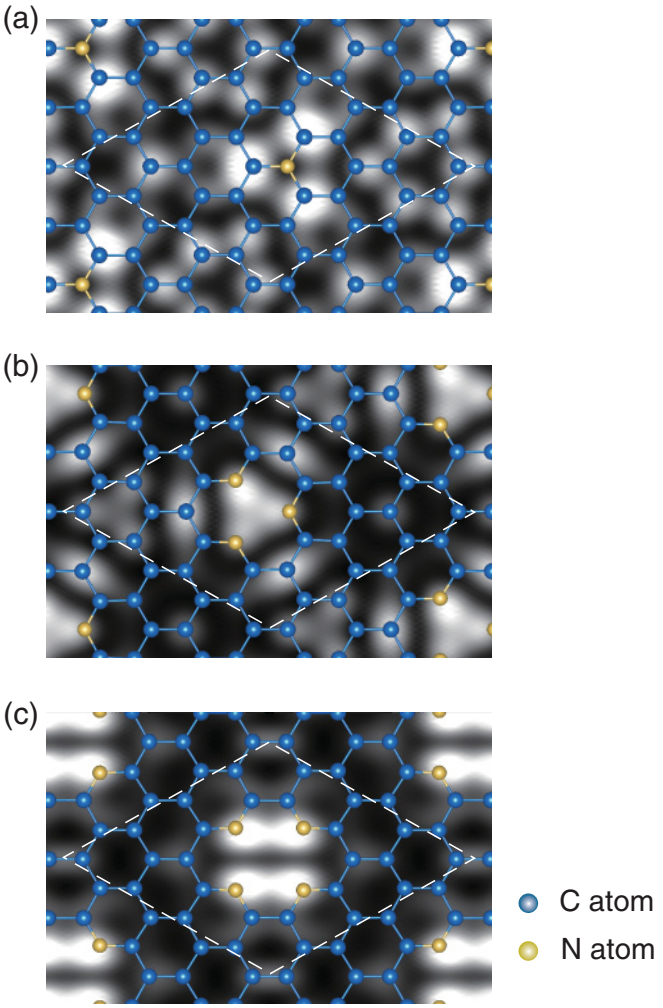

FIG. 5. (Color online) Simulated STM images of N-doped graphenes with (a) substitutional nitrogen and (b) trimerized and (c) tetramerized pyridine-type defects. The STM images are generated at applied bias voltages of (a) +0.5, (b) −0.5, and (c) −0.5 eV. The maximal height of corrugations in the STM images is set to be approximately 5 Å above the graphene sheet. The dashed lines show the supercell.

extends above the N atom as well [Fig. 2(b)]. This discrepancy comes from how the distributions of the LDOSs protrude above the N atom and the surrounding three C atoms: the LDOSs above the three C atoms are more delocalized than that above the N atom. Consequently, the STM image at the three C atoms near the N atom shows three bright spots, whereas the STM image at the N atom appears to be dark.

The STM image of graphene with the trimerized pyridine-type defect at a bias voltage of −0.5 eV (valence band) is shown in Fig. 5(b). The image has three bright spots localized at three N atoms near the carbon vacancy, and it seems to form a triangular hillock since the spatial distribution of the two N-defect states near the Fermi level has *p*-orbital character protruding toward the carbon vacancy [Figs. 3(c) and 3(d)]. In addition, the STM image exhibits oscillations of electron density with C_3 symmetry propagating outward from the center of the vacancy. Similar features are also observed in the case of a point defect in graphite surfaces and graphene.[21,30,31]

Finally, we show in Fig. 5(c) the STM image of tetramerized pyridine-type defects in graphene. In this STM image, there are two large oval-shaped protrusions consisting of four bright spots located at N atoms because the p-orbital-shaped electron density of the N atoms protrudes toward the carbon vacancy [Fig. 4(b)]. Similar oval-shaped protrusions rotated by $\pi/2$ compared with those in Fig. 5(c) have been reported,[21] corresponding to the pentagon-octagon-pentagon structure in Fig. 1(g).

IV. SUMMARY

Based on first-principles total-energy calculations, we have studied the atomic structures, energetics, and electronic properties of various N-doping configurations in graphene. The formation-energy calculations indicate that the substitutional nitrogen defect has the lowest energy among the possible N-doped defects in graphene. The present relative energy calculations reveal that the pyridine-type defects are energetically favored rather than the substitutional nitrogen defect under the existence of a vacancy in graphene. In addition, both the trimerized and the tetramerized pyridine-type defects in graphene are expected to be plausible atomic configurations among nitrogen-vacancy complexes due to the small difference in their formation energies. We have calculated the electronic structures of several N-doped configurations in graphene. It is found that impurity-induced states appear around the Fermi level and show the spatial distributions of electron densities localized around nitrogen defects. We have also calculated STM images of substitutional nitrogen and trimerized and tetramerized pyridine-type defects in graphene. The simulated STM images exhibit distinctive corrugations, depending strongly on the atomic configurations of the nitrogen defects. They are of great importance in future STM experiments for identifying N-doped configurations.

ACKNOWLEDGMENTS

This work was partly supported by the Global Center of Excellence Program of MEXT, Japan through the Nanoscience and Quantum Physics Project of the Tokyo Institute of Technology, a Grant-in-Aid for Scientific Research on Priority Areas of MEXT Japan, the"Carbon Nanotube Nano-Electronics" Project, and the Elements of Science and Technology Project of MEXT Japan. Computations were done at the Institute for Solid State Physics, the University of Tokyo, at the Global Scientific Information and Computing Center of the Tokyo Institute of Technology, at Cybermedia Center of Osaka University, at Cyberscience Center of Tohoku University, and at the Research Center for Computational Science of the National Institutes of Natural Sciences.

[1] N. H. Shon and T. Ando, J. Phys. Soc. Jpn. **67**, 2421 (1998).
[2] K. S. Novoselov, A. K. Geim, S. V. Morozov, D. Jiang, Y. Zhang, S. V. Dubonos, I. V. Grigorieva, and A. A. Firsov, Science **306**, 666 (2004).
[3] S. V. Morozov, K. S. Novoselov, M. I. Katsnelson, F. Schedin, D. C. Elias, J. A. Jaszczak, and A. K. Geim, Phys. Rev. Lett. **100**, 016602 (2008).
[4] A. K. Geim and K. S. Novoselov, Nat. Mater. **6**, 183 (2007).
[5] K. Prassides, K. M. Keshavarz, J. C. Hummelen, W. Andreoni, P. Giannozzi, E. Beer, C. Bellavia, L. Cristofolini, R. Gonzalez, A. Lappas, Y. Murata, M. Malecki, V. Srdanov, and F. Wudi, Science **271**, 5257 (1996).
[6] S. C. Erwin and W. E. Pickett, Phys. Rev. B **42**, 11056 (1990).
[7] D. Wei, Y. Liu, Y. Wang, H. Zhang, L. Huang, and G. Yu, Nano Lett. **9**, 1752 (2009).
[8] Y.-C. Lin, C.-Y. Lin, and P.-W. Chiu, Appl. Phys. Lett. **96**, 133110 (2010).
[9] P. Ayala, A. Grüneis, T. Gemming, D. Grimm, C. Kramberger, M. H. Rümmeli, L. Freire Jr., H. Kuzmany, R. Pfeiffer, A. Barreiro, B. Büchner, and T. Pichler, J. Phys. Chem. C **111**, 2879 (2007).
[10] B. Guo, Q. Liu, E. Chen, H. Zhu, L. Fang, and J. R. Gong, Nano Lett. **10**, 4975 (2010).
[11] I. C. Gerber, P. Puech, A. Gannouni, and W. Bacsa, Phys. Rev. B **79**, 075423 (2009).
[12] Y. Fujimoto and S. Saito, Physica E **43**, 677 (2011).
[13] To check the size of the supercell of graphene, we calculated the formation energy of the tetramerized pyridine-type graphene [Fig. 1(e)] with a larger 5×5 supercell. The difference of the formation energies between the 4×4 and the larger 5×5 supercells is found to be only 0.014 eV. Therefore, the 4×4 supercell should give qualitatively the same results as the larger supercell.
[14] P. Hohenberg and W. Kohn, Phys. Rev. **136**, B864 (1964).
[15] N. Troullier and J. L. Martins, Phys. Rev. B **43**, 1993 (1991).
[16] W. Kohn and L. J. Sham, Phys. Rev. **140**, A1133 (1965).
[17] D. M. Ceperley and B. J. Alder, Phys. Rev. Lett. **45**, 566 (1980); J. P. Perdew and A. Zunger, Phys. Rev. B **23**, 5048 (1981).
[18] Computations have been performed using the Tokyo *Ab Initio* Program Package (TAPP) which was developed by a consortium initiated at the University of Tokyo: J. Yamauchi, M. Tsukada, S. Watanabe, and O. Sugino, Phys. Rev. B **54**, 5586 (1996); H. Kageshima and K. Shiraishi, *ibid.* **56**, 14985 (1997); O. Sugino and A. Oshiyama, Phys. Rev. Lett. **68**, 1858 (1992).
[19] J. Tersoff and D. R. Hamann, Phys. Rev. B **31**, 805 (1985).
[20] H. Okada, Y. Fujimoto, K. Endo, K. Hirose, and Y. Mori, Phys. Rev. B **63**, 195324 (2001); Y. Fujimoto, H. Okada, K. Endo, T. Ono, S. Tsukamoto, and K. Hirose, Mater. Trans. **42**, 2247 (2001); S. Berber and A. Oshiyama, Phys. Rev. B **77**, 165405 (2008); Y. Fujimoto and A. Oshiyama, *ibid.* **81**, 205309 (2010).
[21] H. Amara, S. Latil, V. Meunier, Ph. Lambin, and J.-C. Charlier, Phys. Rev. B **76**, 115423 (2007).
[22] A. A. El-Barbary, R. H. Telling, C. P. Ewels, M. I. Heggie, and P. R. Briddon, Phys. Rev. B **68**, 144107 (2003).
[23] B. Zheng, P. Hermet, and L. Henrard, ACS Nano **4**, 4165 (2010).
[24] J. Ito, J. Nakamura, and A. Natori, J. Appl. Phys. **103**, 113712 (2008).
[25] K. Kanamitsu and S. Saito, J. Phys. Soc. Jpn. **71**, 483 (2002).
[26] K. E. Kweon and G. S. Hwang, Phys. Rev. B **82**, 195439 (2010).
[27] Y. F. Li, Z. Zhou, and L. B. Wang, J. Chem. Phys. **129**, 104703 (2008).
[28] E. C. Silva, F. L. Urias, E. M. Sandoval, B. G. Sumpter, H. Terrones, J. C. Charlier, V. Meunier, and M. Terrones, ACS Nano **3**, 1913 (2009).

[29]E. G. Espino, F. L. Urias, H. Terrones, and M. Terrones, Mater. Express **1**, 127 (2011).
[30]K. F. Kelly and N. J. Halas, Surf. Sci. **416**, L1085 (1998).
[31]T. Kondo, Y. Honma, J. Oh, T. Machida, and J. Nakamura, Phys. Rev. B **82**, 153414 (2010).
[32]O. V. Yazyev and L. Helm, Phys. Rev. B **75**, 125408 (2007).
[33]S. Caslo, O. M. Løwik, R. Martinazzo, and G. F. Tantardini, J. Chem. Phys. **130**, 054704 (2009).
[34]T. O. Wehling, A. V. Balatsky, M. I. Katsnelson, A. I. Lichtenstein, K. Scharnberg, and R. Wiesendanger, Phys. Rev. B **75**, 125425 (2007).